Supplementary Information for

Proteostasis collapse is a driver of cell aging and death

Mantu Santra, Ken A. Dill and Adam M.R. de Graff

Corresponding Ken A. Dill.
E-mail: dill@laufercenter.org

Supporting Information Text

The NUMA model of proteostasis collapse in cell aging

Chaperones maintain proteins and proteomes in highly folded states by binding non-native conformations at their exposed hydrophobic regions and providing them with a faster route to folding (1). However, damaged and destabilized proteins, which have problems folding, are known to bind to chaperones much more frequently (2), thus decreasing chaperone availability for undamaged proteins and potentially leading to proteostasis collapse. The NUMA model is a minimal model that captures these behaviors.

Figure 1 depicts our model. It has two planes of folding dynamics, one for undamaged protein (the top panel) and a second for damaged protein (the bottom panel). First, here's a brief summary. Undamaged proteins flow within the undamaged plane as they fold and unfold, are trafficked through chaperone, or degrade or aggregate. The undamaged plane rate parameters are given in Table S1. Damage can occur, causing an unfolded protein from the undamaged plane to transition irreversibly to the damaged plane. Once a protein enters the damaged plane, it traffics in that plane with all the same rate parameters as it would have had in the undamaged plane, except for one difference: damaged proteins are unable to fold. This is due to the loss of stability suggested by experiment (3) and theory (4) upon modification of a single side chain, the most frequent form of oxidation (Table S1). Therefore, damaged protein can either aggregate via misfolding or be degraded.

The central point of the two-plane dynamics is to express how damage events slowly and irretrievably destabilize the folding of the proteome as the cell ages. In addition, the model supposes that this has functional consequences. Biologically, damaged proteins hinder the cell through two parallel mechanisms: (i) loss of protein function and (ii) destabilization of the proteome resulting in chaperone titration and aggregation, collectively creating a gain of toxic function. The NUMA model specifically focuses on the effect of destabilization, not the loss of function. The time-dependent populations of each conformational state of the NUMA model are given in the Equations section.

Age dependence of cell growth and protein degradation

The rates of cell growth $k_{gr}(t)$ and protein degradation $k_{deg}(t)$ change with age, t. These dynamics play important roles in proteostasis collapse, as they constrain the rate at which proteins are turned over and hence the rate at which damage is diluted (growth) or cleared (degradation). But, rather than attempt to model the origins of the age dependence of $k_{gr}(t)$ and $k_{deg}(t)$ - which may reflect a complex trade-off between reproductive yield and longevity regulated by the germline - here we simply take their experimental values at $20°C$ as inputs and explore their consequences on proteostasis collapse (5). The data used is shown in Fig. S1 and is approximated by an exponential function.

Folding, misfolding, aggregation, chaperoning and damage. Understanding the principles of proteostasis requires consideration of the timescales of its processes. In our model, we have coarse-grained the folding landscape into several critical states, namely those that are functional and native (N), unfolded (U), misfolded (M) and aggregated (A), as shown in Fig. 1. We assign transition rates between these states that reflect typical values across the experimental literature. Here, we discuss the sources.

Stability of the native state. The folding stability, ΔG, of a protein has been shown both experimentally and theoretically to depend on many factors, including hydrophobicity and chain length (6). Folding stability is also highly temperature-dependent, having a roughly inverted parabolic relationship that becomes zero at the hot and cold denaturation points of roughly $50°C$ and $-20°C$, respectively, and reaches a typical peak stability $\Delta G_{max} \approx 10\ kT$ at intermediate temperatures $T_{\Delta G_{max}} \approx 10 - 20°C$ (7). This can be expressed as

$$\Delta G = \Delta G_{max}\left[1 - \frac{(T - T_{\Delta G_{max}})^2}{(T_{melt} - T_{\Delta G_{max}})^2}\right] \tag{S1}$$

where the values of ΔG_{max}, $T_{\Delta G_{max}}$ and T_{melt} (hot denaturation) are given in Table S1.

Unfolding. Proteins have finite stability and are prone to spontaneous unfolding, even when in their native conformation. The rate of this unfolding, k_u, has been determined experimentally using a number of approaches that suggest, for small proteins, an unfolding barrier with an activation energy E_a of roughly $100 kJ/mol$ [8]. Using the Arrhenius equation

$$k_u = k_{u,o} \; e^{-E_a/RT} \tag{S2}$$

relating the barrier crossing rate to the standard attempt frequency $k_{u,o} = 6.2 \times 10^{12} \; s^{-1}$ gives $k_u \approx 1 \; d^{-1}$ (at $20°C$). Given that proteins typically form protein-protein complexes with a mildly stabilizing effect [9], the estimate of $k_u \approx 1 \; d^{-1}$ serves as an upper limit for the average unfolding rate. We found an unfolding rate of $0.4 \; d^{-1}$ at $20°C$ provides dynamics close to experimental data when used in combination with experimental HSP70 concentrations (Table S1).

Folding. The folding rate, k_f, can be determined from the unfolding rate and the folding stability according to

$$k_f = k_u \; e^{\Delta G/RT} \tag{S3}$$

At $20°C$, near the peak stability, an unfolding rate $k_u = 0.4 \; d^{-1}$ and folding stability $\Delta G = 24.5 \; kJ/mol$ give a folding rate $k_f = 0.1 \; s^{-1}$ that corresponds to a folding time of roughly 5-10 seconds. This is comparable to the estimated cycle time of the eukaryotic HSP70 (see Chaperoning in SI).

Misfolding. Proteins that require the help of foldases are characterized by high rates of misfolding, k_{um}, that greatly exceed the rate of proper folding [10], due in part to the higher number of possible misfolding states. These proteins therefore require many chaperone binding events to fold. We assume here that misfolding is 30 times faster than folding, *i.e.* $k_{um} = 30 \; k_f$, consistent with the high number of chaperone-mediated folding cycles required for folding, as inferred in previous studies [1].

Unmisfolding. We assume that misfolded proteins have comparable folding stability to native proteins. Thus, a similar relation to that in Eq.S3 can be written for the misfolded state. The sole difference is the 30-fold faster inter-conversion between misfolded and unfolded structures due to the 30-fold faster misfolding rate compared to the folding rate. The unmisfolding rate can thus be written as $k_{mu} = 30 \; k_u$. This rate, amounting to once every 2 hours (for $k_u = 0.4 \; d^{-1}$), is much slower than the rate at which an HSP70 would detect and bind the non-native protein (Table S1), and thus does not serve as a major route to refolding.

Aggregation. The aggregation process is modeled by two-step Finke-Watzky type kinetics [11]. The nucleation kinetics are considered to be a binary collision process where two misfolded proteins collide and form aggregate. This binary-collision model gives a nucleation flux $k_a[M]^2$. The value of k_a is chosen to be comparable to the experimental values, but is not tightly constrained by the available data. The growth is treated similar to nucleation where two molecules collide and form aggregate, except that in this case one of the molecules is already aggregated (A). In other words, aggregates catalyze the conversion of misfolded proteins to aggregate with a flux $k_g[M][A]$.

Degradation. Proteins in their non-native states are more prone to degradation compared to their native counterpart. It involves multiple steps involving binding of proteins by ubiquitin and then, with the help of ATP, the proteins are degraded into either small peptides or amino acids. The degradation in our model is simple; it approximates the whole process by single-step first order kinetics where the flux of degradation is proportional to the concentration of degradable protein: $k_{deg}[P]$ (Fig. 1). The rate constant of degradation used in the model is given in Table S1.

Chaperoning. There are multiple chaperones in *C. elegans*. Even in simple organisms, such as *E. Coli*, there are three major chaperones: trigger factor (TF), DnaK/J/GrpE (KJE or HSP70) and GroEL/S (GroE or HSP60). The mechanism of chaperoning is highly complex. Although all the chaperones help the client proteins in their folding pathways, the mechanism as well as the efficiency of their actions are different. Similar to *E. coli*, the cells in *C. elegans* also synthesize HSP70- and HSP60-class chaperones which are conserved in both structure and function. Per complex, previous studies found HSP60 to be more efficient in folding a misfolded protein compared to HSP70. In contrast, due in part to its higher chaperoning rate per unit mass, HSP70 was found to be the most critical chaperone in preventing protein damage, which is a potential threat in cell aging [12]. In our current study, we thus consider only HSP70 chaperone and its simplified kinetics through which it folds its non-native client proteins. The kinetics follow a two-step process whereby the HSP70 binds the non-native client and then releases it to either a native or non-native state based on the rates folding and misfolding.

Chaperone kinetics and binding affinities were estimated from experiments. We take chaperone kinetics to be roughly an order of magnitude slower than those found in well-studied prokaryotes like *E. coli* [1, 10] (Table S1). The slower kinetics reflect the difference in speed observed between prokaryotic and eukaryotic chaperones, which may be a response to the slower natural folding rate of eukaryotic proteins due to their longer average chain length [13, 14]. Proteins that do not require chaperones to fold are not modeled here, as they are predicted to fold too quickly to suffer significant aggregation [1] or damage [12], and thus are not expected to be as sensitive to the slowing protein turnover rates associated with aging, nor play a central role in proteostasis decline.

Mantu Santra, Ken A. Dill and Adam M.R. de Graff

Protein damage. In our model, oxidative damage is assumed to occur only to unfolded proteins. Proteins are unfolded several times during their existence – upon being synthesized and when unfolding spontaneously due to their finite stability. The damage rate is given by $k_{dam} = k_{dam}^o[U]$, with $k_{dam}^o = 0.012 \ s^{-1}$ (Table S1). Given that damage is modeled as occurring only to undamaged protein, it is the ratio of k_{dam}^o to the protective mechanisms of chaperone binding, folding and misfolding that determines the fraction of proteins that become damaged during post-synthesis folding or upon spontaneous unfolding.

Proteomes are susceptible to heat and oxidative damage

While models of proteostasis commonly include interactions between folding non-native proteins and chaperones (1, 14, 15), as captured by the top plane in Fig. 1, our approach is unique in two major respects. First, our model captures the biophysical dependencies that control the sensitivity of protein conformation to changes in temperature and, in turn, the differential sensitivity of conformations to oxidative damage (4, 7, 12). While proteins are often assumed to be highly stable, experiments have shown that they unfold spontaneously on timescales of hours to days. Thus, while our proteostasis model averages over the protein-to-protein heterogeneity within a proteome by modeling a single average protein, it captures the biophysical properties shared across proteomes that dictate their common response to temperature and oxidation and - we hypothesize - controls lifespan.

Heat stress. Temperature affects the dynamics of proteostasis in multiple ways. First, it is a general property of enzymes that their rates increase with temperature following Arrhenius behavior (7, 16). This can be written as

$$k_{cat}^o = k_{cat,o} \ e^{-E_1/RT} \tag{S4}$$

where $k_{cat,o}$ is the catalytic rate in the high-temperature limit. Protein degradation and chaperoning activities are assumed to follow Eq.S4.

While the concerted increase in catalytic rates given by Eq.S4 has often been cited as predicting a corresponding shortening in lifespan, in line with the Rate-of-Living Hypothesis (17), this conclusion is not necessarily justified. The reason is that not all processes scale at the same rate with temperature. Specifically, protein unfolding grows much more rapidly with temperature than any of the proteostasis mechanisms to counteract it, roughly doubling with every $4°C$ increase in temperature (18, 19). Due to this more rapid increase, the folding burden of a cell shifts from primarily folding newly synthesized proteins at low temperatures to refolding spontaneously unfolded protein at high temperatures (Fig. 3D). As an attempt to cope with the increasing unfolding burden, cells decrease growth rates at high temperatures (Fig. S2). Thus, unlike the Arrhenius temperature dependence of other biological processes, the growth rate follows a non-Arrhenius behavior at high temperature.

$$k_{gr}^o = \frac{k_{gr,o}}{\left[e^{E_1/RT} + e^{(A-E_2/RT)}\right]} \tag{S5}$$

The present study accounts for these different temperature dependencies (Eqs.S4-S5) and predicts their consequences on lifespan (Fig. 3).

Oxidative stress. Figure 4A shows how lifespan depends on the concentration of the oxidant tBuOOH, which is assumed here to create a proportional amount of ROS. This can be expressed by writing the rate constant of damage as

$$k_{dam} = k_{dam}^o \left(1 + \frac{[tBuOOH]}{c_o}\right) \tag{S6}$$

where c_o is fitting parameter corresponding to the concentration of $tBuOOH$ at which the damage rate is double its basal, physiological value. A value of $c_o = 0.5 \ mM$ is used here (Table S1).

Mortality rate and survival probability

The progressive accumulation of damaged protein with age has been widely observed across species (4). Thus, the extent of damage is considered a general biomarker of aging. Many studies in wild-type and mutant *C. elegans* have revealed that the extent of damage in short-lived mutants are almost universally higher than their long-lived counterparts (20), with the few exceptions potentially resulting from the low solubility of the damaged proteins (21). Given that toxicity is commonly believed to arise from oligomers several protein molecules in size – with oxidized proteins being particularly toxic (22, 23) – we model mortality rate $\mu(t)$ in terms of the fraction of protein that is damaged, $f_D(t)$, namely

$$\mu(t) = \mu_o f_D(t)^\alpha \tag{S7}$$

Both α, which determines the non-linear, cooperative nature of the toxicity, and μ_o, its overall scale, are determined from the slope and magnitude of the experimental mortality curve at $20.1°C$ (Fig. 2C, black circles). The values of μ_o and α are reported in Table S1. Interestingly, the value of α is close to the value found in a previous study to capture the relationships between damage level and the rate of mortality and mutation rates ($\alpha \approx 5 - 10$) in irradiated bacteria (22). The mortality rates at other temperatures are predicted using the same values of α and μ_o as at $20.1°C$. From the mortality rate $\mu(t)$, the survival probability $S(t)$ is obtained by using following relation:

$$S(t) = e^{-\int_0^t dt \ \mu(t)} \tag{S8}$$

Tests of assumptions, sensitivities, and factors deliberately left out of the model

Damaged protein. Our model assumes that damaged proteins are not able to fold, and thus are trapped in aggregation-prone conformations. While this is true for heavily damaged proteins, those with only a single oxidized side chain are more likely to be only mildly destabilized by 1-2 $kcal/mol$, comparable to that observed with single point mutations (4). While we chose not to allow folding of damaged proteins to be consistent with past work (12), future models could explore the response to partial destabilization from oxidation. A destabilized, rather than fully blocked, native state would be expected to result in greater accumulation of damaged protein than in the present model. It would also allow loss of function to be explicitly modeled, which was not the focus of the present work.

Mortality. Our model assumes that mortality scales as a power law with the amount of oxidative damage to proteins. While damage-centric theories of aging have been supported by many lines of evidence (24), some observations are claimed to contradict it. Most notably, mutant worms have been found that display heightened damage with no change, or even slight increases, in lifespan (25). Higher levels of damage have also been observed in some long-lived organisms like the naked mole-rat (21) and deer mouse (26). However, two key points may resolve these apparent contradictions. First, in the case of the naked mole-rat, further investigation found that the high damage levels were limited to only a few highly abundant proteins, and thus uncharacteristic of the proteome (21). Second, the higher chaperone content is strongly associated with long-lived organisms (27) and may increase youthful damage levels by keeping mildly oxidized proteins folded and phenotypically silent, buffering the cell from their negative consequences in a manner analogous to that proposed by Susan Lindquist for point mutants (2). Indeed, soluble damage levels of young animals are not good predictors of the longevity of a species (21), even if total damage levels are predictive of impending death (4, 24, 28).

To test whether the model predictions are sensitive to the exact nature of the toxic species, we reran our simulations taking only oxidized aggregates as the cause of mortality. While the temperature and oxidant dependence of lifespan changed modestly, the major findings remain the same. The most important fact is that the Gompertzian behavior of mortality remains the same (Fig. 2C). Human diseases too follow a Gompertzian trend, suggesting a similar underlying mechanism. Whereas some diseases are caused by frailties of particular proteins, aging may result from the system-wide frailty of the whole proteome.

Effective parameters. A key goal of constructing simplified biological models is to identify the minimal set of parameters needed to capture observed behavior. While the number of model parameters, summarized in Table S1, is by no means small, they coalesce into a much smaller set of effective parameters that dictate the model behavior explored in this work. Two effective parameters predominate.

The first is chaperone capacity relative to basal requirements (the fold-surplus). This effective parameter is determined by chaperone concentration, chaperone kinetics, and protein stability. Our estimates suggest a roughly 5-fold spare capacity at $20°C$ (8 μM out of 45 μM of chaperone is bound to non-native protein), as summarized in Fig. S3. This spare capacity is reasonable, given that: (i) the spare capacity of another key chaperone system, HSP90, is also expressed at least 5- to 10-fold beyond the minimum requirements for growth (29), and (ii) a 5-fold spare capacity allows roughly two $8°C$ doublings in unfolding rate before there is no capacity left to fold newly translated protein, consistent with sythesis rates plummeting around $35°C$ (Fig. S2). This spare capacity is not wasted at lower temperatures, however, as it determines the time an unfolded, damage-prone protein needs to wait for help, which has previously been shown to affect damage levels (12, 30). The net result of this effective parameter is to determing the temperature at which lifespan begins to deviate strongly from the Arrhenius rate-of-living expectation, shown in Fig. 3A and 3C. The rapid decline beyond $28°C$ therefore constrains our model and informs us on mechanism, rather than being an independent model prediction.

The second effective parameter is the damage rate relative to a protein's dwell time in the unfolded state. This quantity is more meaningful to model behavior than the damage rate alone, which is poorly characterized and certain to vary greatly between proteins. Importantly, this effective parameter determines the degree of chaperone titration by damaged proteins. While not known exactly experimentally, chaperone titration by damaged protein has been shown to significantly amplify induction of the heat shock response (which senses chaperone titration). By running our model with and without the ability of damaged proteins to bind chaperes, we demonstrated that our effective parameter value is sufficient to moderately affect sensitivity to chaperone or proteasome expression levels (Figs. 5B and 6B). These predictions serve to motivate future experimental testing.

Potential improvements. Here are some potential sources of future improvements to the model. (i) We model a single ATP-dependent folding mechanism representing HSP70-class chaperones. In reality, proteins are folded through a cooperative network of several ATP-dependent chaperone classes, as explored previously in *E. coli* (1). While the overall network behavior can likely be captured to a first approximation by an effective folding capacity similar to the one explored here, the relative importance of upstream (HSP70) and downstream (HSP90) chaperoning on proteome health and longevity is worth exploring. (ii) Small heat-shock proteins are not currently treated. One possible consequence of their absence from our model is a lower effective solubility of damaged proteins and, as a result, a lower predicted level of soluble damaged protein (Fig. 2B). (iii) We have not modeled the clearance of aggregates, which will be particularly important when modeling organisms with lifespans considerably longer than the typical protein half-life. (iv) Degradation of soluble proteins is treated quite simply here (Fig. 1) due to limitations in the current understanding of factors determining protein half-life. However, the triage decision of whether to refold or degrade an unfolded protein, and thus the trade-off between maximizing yield vs. minimizing damage, poses an interesting topic for exploration. (v) We have made the simplifying approximation that the decay constants controlling the

Mantu Santra, Ken A. Dill and Adam M.R. de Graff

age-dependence of growth and degradation are ROS-independent. Future models should aim to derive these decay constants from first principles based, for example, on the degree of chaperone titration. Such a treatment could also seek to explore how the exponential decay in growth and degradation rates even under standard conditons may arise from an evolutionary optimization of reproductive fitness for a given resource availability.

Equations

Undamaged protein

$$\frac{d[N]}{dt} = k_f[U] + \frac{k_{ce}\ k_f[CU]}{k_{ce} + k_{um} + k_f} - (k_{gr} + k_u)[N] \tag{S9}$$

$$\frac{d[U]}{dt} = k_{gr}[P] + \frac{k_{ce}^2\ [CU]}{k_{ce} + k_{um} + k_f} + k_{mu}[M] + k_u[N] + k_{deg}([M] + [M_{ox}] + [U_{ox}]) - k_{dam}[U]$$
$$- (k_f + k_{um} + k_{gr} + k_{cb}[C])[U] \tag{S10}$$

$$\frac{d[M]}{dt} = \frac{k_{ce}\ k_{um}[CU]}{k_{ce} + k_{um} + k_f} + k_{um}[U] - (k_{gr} + k_{mu} + k_{deg} + k_{cb}[C])[M] - (k_g([A] + [A_{ox}]) + 2k_a([M] + [M_{ox}]))[M] \tag{S11}$$

$$\frac{d[A]}{dt} = -k_{gr}[A] + (k_g[A] + k_g[A_{ox}] + 2\ k_a[M] + 2\ k_a[M_{ox}])[M] \tag{S12}$$

Damaged protein

$$\frac{d[U_{ox}]}{dt} = k_{gr}[P] + \frac{k_{ce}^2\ [CU_{ox}]}{k_{ce} + k_{um}} + k_{mu}[M_{ox}] + k_{dam}[U] - (k_f + k_{um} + k_{gr} + k_{deg} + k_{cb}[C])[U_{ox}] \tag{S13}$$

$$\frac{d[M_{ox}]}{dt} = \frac{k_{ce}\ k_{um}[CU_{ox}]}{k_{ce} + k_{um}} + k_{um}[U_{ox}] - (k_{gr} + k_{mu} + k_{deg} + k_{cb}[C])[M_{ox}] - (k_g([A] + [A_{ox}]) + 2k_a([M] + [M_{ox}]))[M_{ox}] \tag{S14}$$

$$\frac{d[A_{ox}]}{dt} = -k_{gr}[A_{ox}] + (k_g([A] + [A_{ox}]) + 2\ k_a([M] + [M_{ox}]))[M_{ox}] \tag{S15}$$

Chaperoning

$$\frac{d[C]}{dt} = \left(k_{gr} + \frac{k_{ce}^2}{k_{ce} + k_{um} + k_f} + \frac{k_{ce}k_{um}}{k_{ce} + k_{um} + k_f} + \frac{k_{ce}k_f}{k_{ce} + k_{um} + k_f}\right)[CU] + \left(k_{gr} + \frac{k_{ce}^2}{k_{ce} + k_{um}} + \frac{k_{ce}k_{um}}{k_{ce} + k_{um}}\right)[CU_{ox}]$$
$$- k_{cb}([U] + [U_{ox}] + [M] + [M_{ox}])[C] \tag{S16}$$

$$\frac{d[CU]}{dt} = -\left(k_{gr} + \frac{k_{ce}^2}{k_{ce} + k_{um} + k_f} + \frac{k_{ce}k_{um}}{k_{ce} + k_{um} + k_f} + \frac{k_{ce}k_f}{k_{ce} + k_{um} + k_f}\right)[CU] + k_{cb}([U] + [M])[C] \tag{S17}$$

$$\frac{d[CU_{ox}]}{dt} = -\left(k_{gr} + \frac{k_{ce}^2}{k_{ce} + k_{um}} + \frac{k_{ce}k_{um}}{k_{ce} + k_{um}}\right)[CU_{ox}] + k_{cb}([U_{ox}] + [M_{ox}])[C] \tag{S18}$$
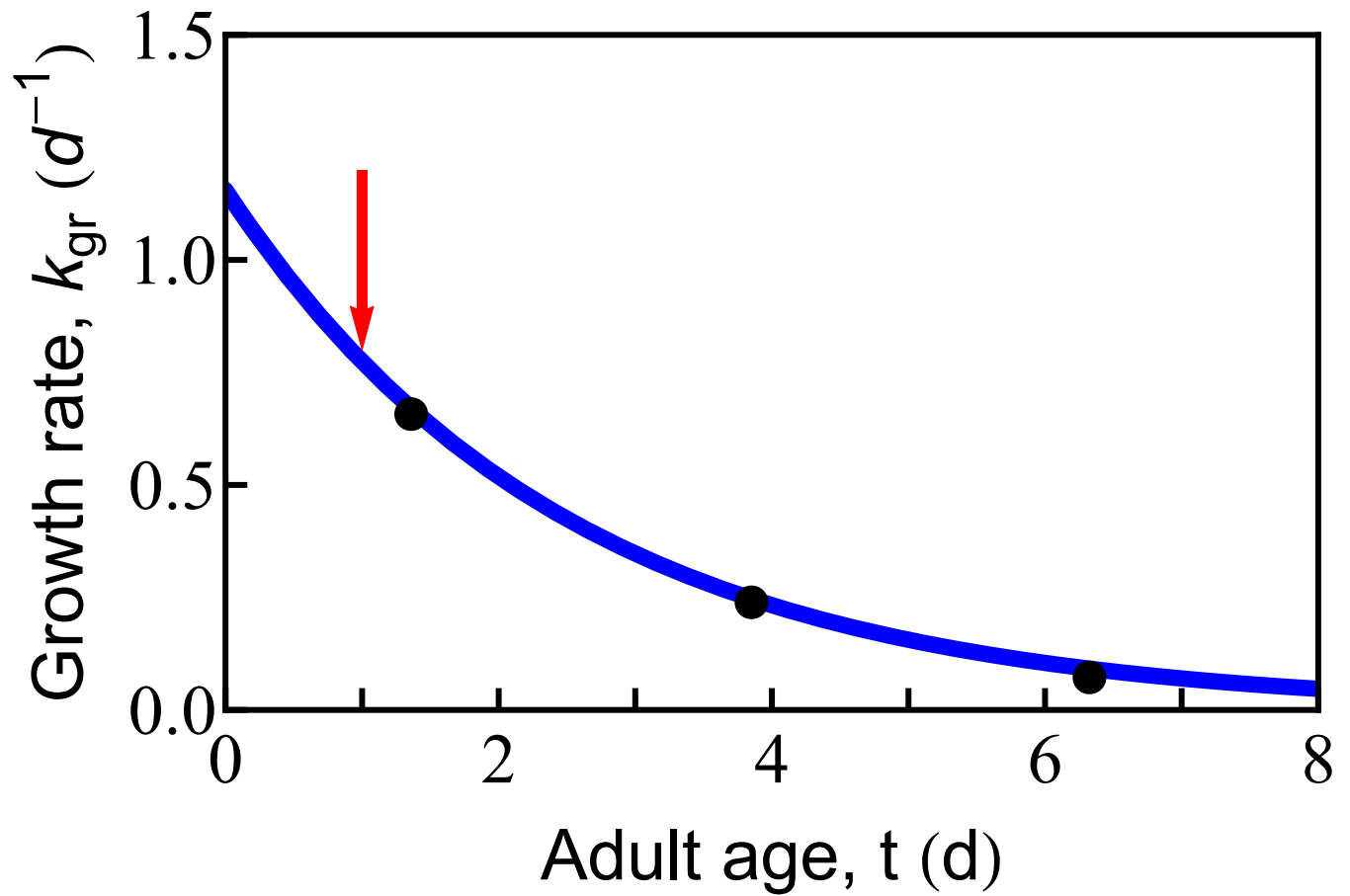
Fig. S1. Growth rate declines markedly with age. The growth rate of wild-type *C. elegans* decays exponentially with age (black circles, extracted from Ref.(5)). The blue line represents the exponential fit to the data, giving a decay constant $\gamma = 0.4 \ d^{-1}$, and is an input in the present study. The red arrow indicates the first day of adulthood and is taken as the starting point in our model.

Mantu Santra, Ken A. Dill and Adam M.R. de Graff
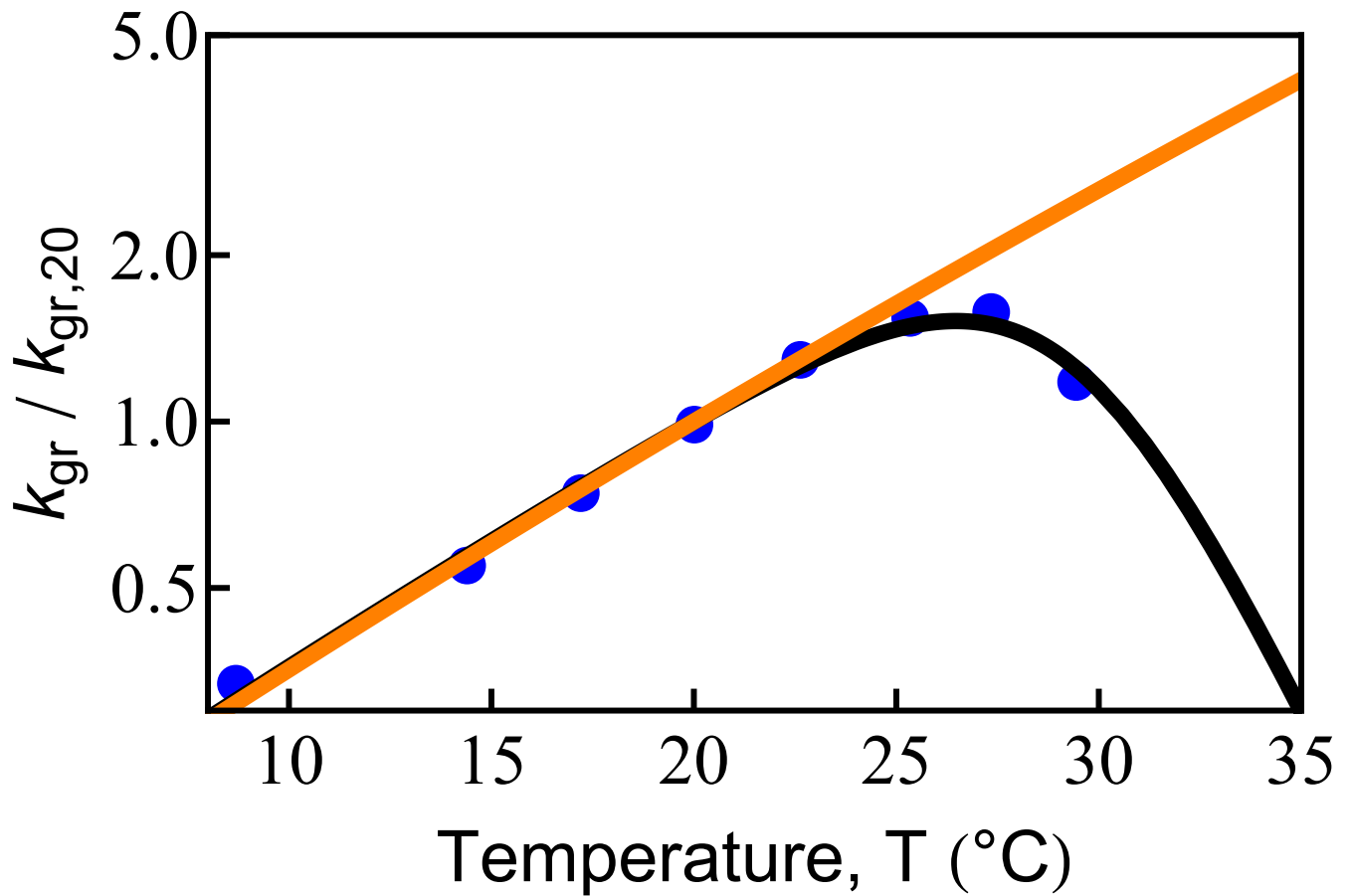
Fig. S2. Growth rate deviates from Arrhenius behavior at high temperature. Experimentally measured growth rates (blue circles) (31) and the corresponding non-Arrhenius fit (black line, Eq. S5) deviate significantly from Arrhenius behavior (orange line) above $28°C$.
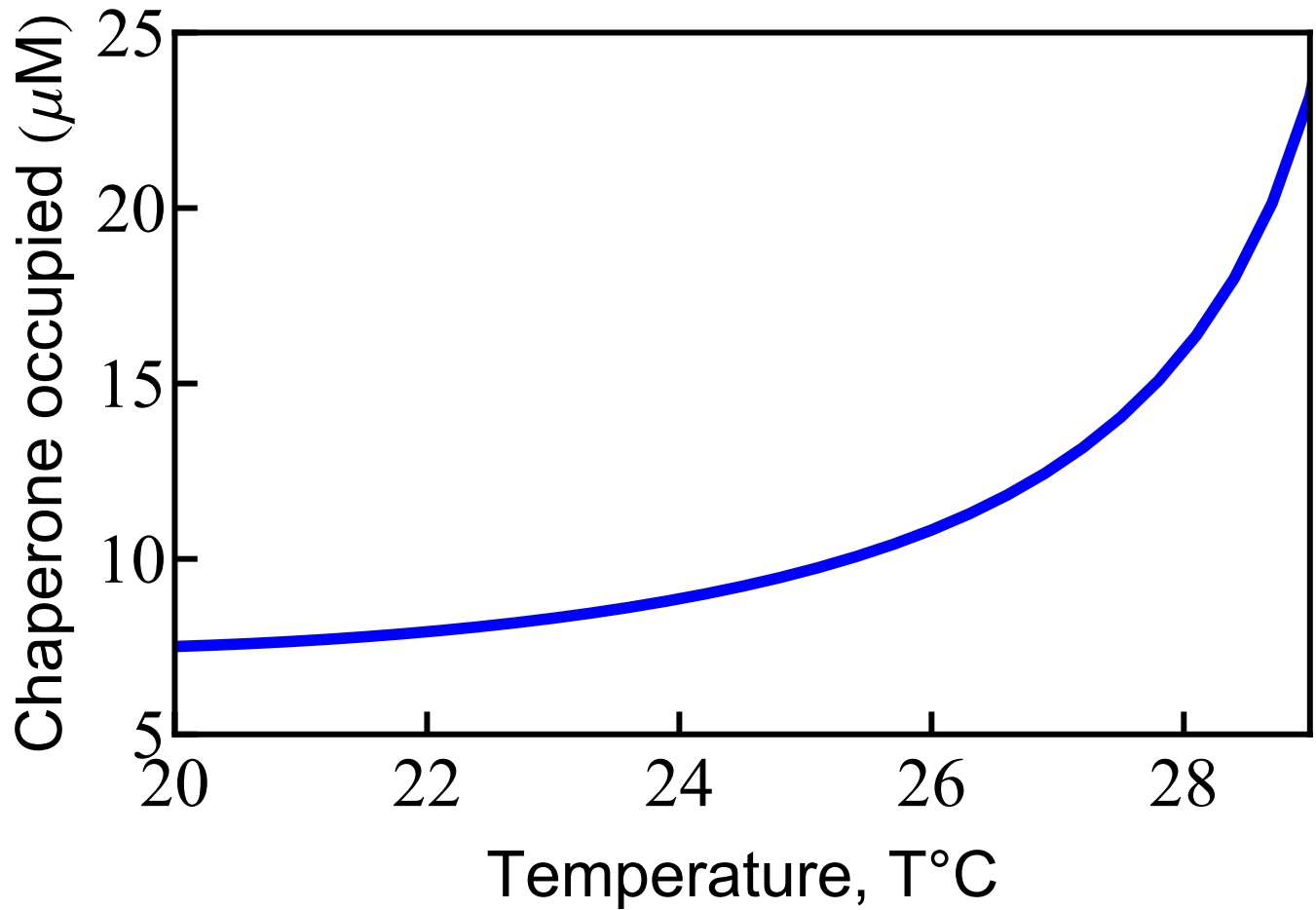
Fig. S3. Chaperone requirements rise rapidly above the temperature of maximum protein stability. As growth temperature deviates from the region of maximum protein stability ($10 - 20^\circ C$), the model predicts a highly non-linear increase in the amount of chaperone required to maintain the same level of proteome foldedness. Total HSP70 chaperone concentration is $45 \ \mu M$ (Table S1).

Mantu Santra, Ken A. Dill and Adam M.R. de Graff
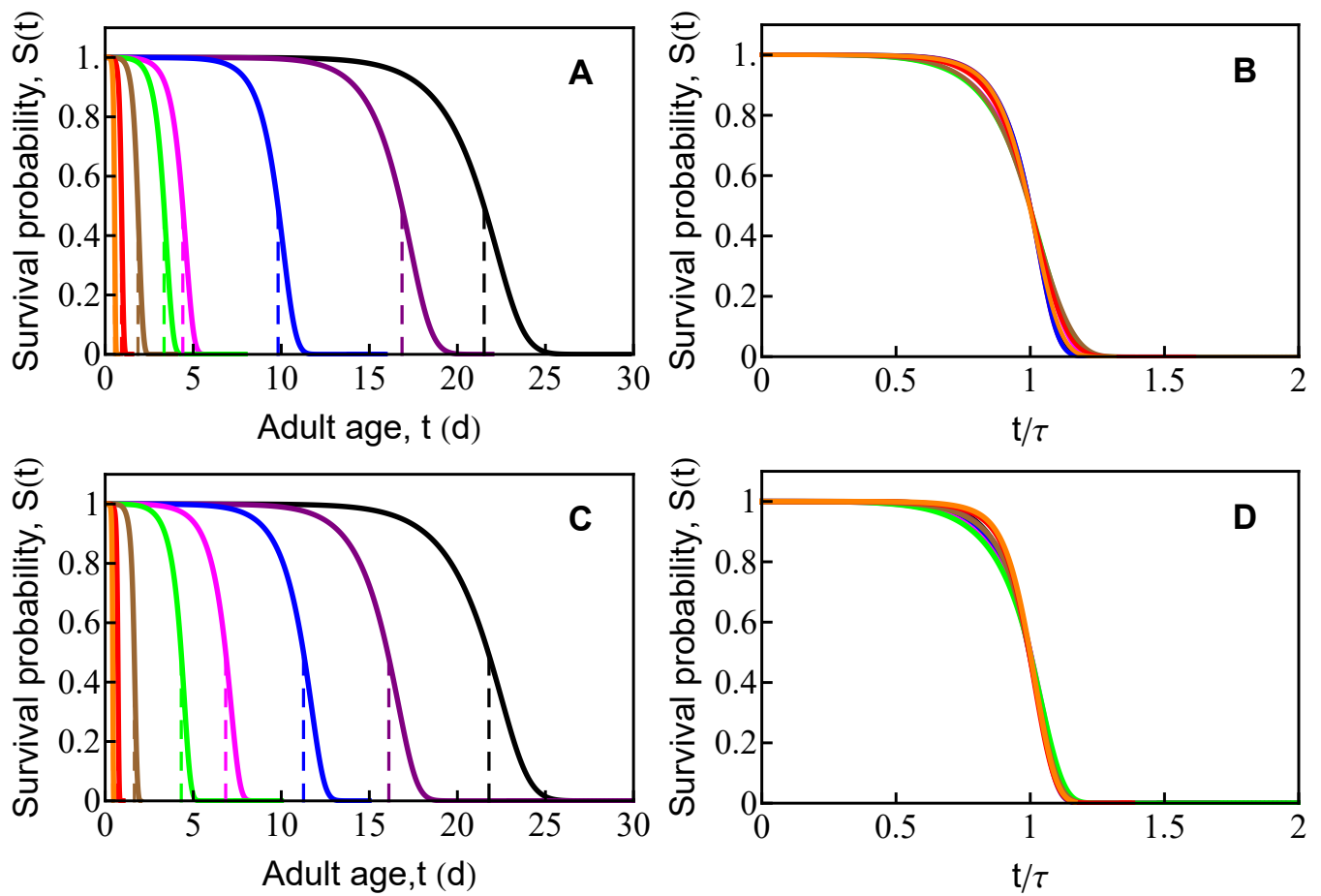
Fig. S4. Scaling of lifespan with temperature and ROS. (A) Predicted survival curves at the same temperatures as the mortality curves in Fig. 3B, namely $20.1°C$, 22.1, 25.5, 28.3, 28.9, 30, 31.3 and $32.4°C$, from black to orange. (B) These survival probabilities, when temporally scaled to the 50% survival time τ, are similar but show a gradual broadening at higher temperature, as observed experimentally (32). (C) and (D) are the same as (A) and (B), respectively, except that ROS level is varied rather than temperature. The concentrations of ROS are, from black to orange, 0 mM, 0.2, 0.5, 1, 1.5, 3, 6, 10 mM.

Table S1. List of Parameters

Parameter	Value	Reference
E_1	$17\ kcal/mol\ (71\ kJ/mol)$	(31)
E_2	$68\ kcal/mol\ (284\ kJ/mol)$	(31)
A	141	(31)
E_a	$30\ kcal/mol\ (125\ kJ/mol)$	(33)
$k_{gr}^o(T = 20°C)$	$1.15\ d^{-1}$	(34)
λ_{gr}	$0.4\ d^{-1}$	(34)
$k_{deg}^o(T = 20°C)$	$3.85\ d^{-1}$	This work
λ_{deg}	$0.14\ d^{-1}$	(34)
$k_u(T = 20°C)$	$0.4\ d^{-1}$	This work
ΔG_{max}	$5.9\ kcal/mol\ (24.5\ kJ/mol)$	(7)
$T_{\Delta G_{max}}$	$18°C$	(7)
T_{melt}	$45°C$	(7, 35)
k_a	$4 \times 10^{-5}\ \mu M^{-1}s^{-1}$	This work
k_g	$2 \times 10^{-2}\ \mu M^{-1}s^{-1}$	This work
k_{cb}	$0.25\ \mu M^{-1}s^{-1}$	This work
$k_{ce}(T = 20°C)$	$0.1\ s^{-1}$	(36)
k_{dam}^o	$0.012\ s^{-1}$	(12)
c_o	$0.5\ mM$	This work
N_p	1500	This work
$[P]$	$1\ \mu M$	(10)
$[C]$	$45\ \mu M$	(37)
μ_o	$9.5 \times 10^{-6}\ d^{-1}$	This work
α	6.4	This work

References

1. Santra M, Farrell D, Dill K (2017) Bacterial proteostasis balances energy and chaperone utilization efficiently. *Proc Natl Acad Sci USA* 114:E2654–E2661.
2. Karras G, et al. (2017) Hsp90 shapes the consequences of human genetic variation. *Cell* 168:856—-866.
3. Tokuriki N, Stricher F, Schymkowitz J, Serrano L, Tawfik D (2007) The stability effects of protein mutations appear to be universally distributed. *Journal of Molecular Biology* 369:1318–1332.
4. de Graff A, Hazoglou M, Dill K (2016) Highly charged proteins: The achilles' heel of aging proteomes. *Structure* 24:329–336.
5. Van Voorhies W, Ward S (1999) Genetic and environmental conditions that increase longevity in caenorhabditis elegans decrease metabolic rate. *Proc. Natl. Acad. Sci. U.S.A.* 96:11399–11403.
6. Ghosh K, de Graff A, Sawle L, Dill K (2016) Role of proteome physical chemistry in cell behavior. *The Journal of Physical Chemistry B* 120:9549–9563.
7. Sawle L, Ghosh K (2011) How do thermophilic proteins and proteomes withstand high temperature? *Biophysical Journal* 101:217–227.
8. Peterson ME, Eisenthal R, Danson MJ, Spence A, Daniel RM (2004) A new intrinsic thermal parameter for enzymes reveals true temperature optima. *The Journal of Biological Chemistry* 279(20):20717–20722.
9. Dixit PD, Maslov S (2013) Evolutionary capacitance and control of protein stability in protein-protein interaction networks. *PLOS Computational Biology* 9(4):1–9.
10. Kerner M, et al. (2005) Proteome-wide analysis of chaperonin-dependent protein folding in escherichia coli. *Cell* 122:209–220.
11. Morris AM, Watzky MA, Finke RG (2009) Protein aggregation kinetics, mechanism, and curve-fitting: A review of the literature. *Biochimica et Biophysica Acta* 1794:375–397.
12. Santra M, Dill K, de Graff A (2018) How do chaperones protect a cell's proteins from oxidative damage? *Cell Systems* 6(6):743–751.
13. Zou T, Williams N, Ozkan SB, Ghosh K (2014) Proteome folding kinetics is limited by protein halflife. *Plos One* 9(11):e112701.
14. Chen K, et al. (2017) Thermosensitivity of growth is determined by chaperone-mediated proteome reallocation. *Proc Natl Acad Sci USA* 114(43):11548–11553.
15. Kirkwood T (2005) Understanding the odd science of aging. *Cell* 120:437–447.
16. Ghosh K, Dill KA (2010) Cellular proteomes have broad distributions of protein stability. *Biophysical Journal* 99:3996–4002.
17. Pearl R (1928) *The rate of living.* (University of London Press Ltd.).
18. Guo M, Xu Y, Gruebele M (2012) Temperature dependence of protein folding kinetics in living cells. *Proc. Natl. Acad. Sci. USA* 109(44):17863—-17867.
19. Holtzer M, et al. (2001) Temperature dependence of the folding and unfolding kinetics of the gcn4 leucine zipper via 13c-nmr. *Biophysical Journal* 80:939–951.
20. Adachi H, Fujiwara Y, Ishii N (1998) Effects of oxygen on protein carbonyl and aging in caenorhabditis elegans mutants with long (age-1) and short (mev-1) life spans. *Journal of Gerontology: Biological Sciences* 53A(4):B240–244.
21. Bhattacharya A, et al. (2011) Attenuation of liver insoluble protein carbonyls: indicator of a longevity determinant? *Aging Cell* 10:720–723.
22. Krisko A, Radman M (2013) Phenotypic and genetic consequences of protein damage. *PLoS Genet* 9(9):e1003810.
23. Radman M (2016) Protein damage, radiation sensitivity and aging. *DNA Repair* 44:186–192.
24. Krisko A, Radman M (2019) Protein damage, ageing and age-related diseases. *Open Biology* 9(3):180249.
25. Van Raamsdonk JM, Hekimi S (2009) Deletion of the mitochondrial superoxide dismutase sod-2 extends lifespan in caenorhabditis elegans. *Plos Genetics* 5:e1000361.
26. Shi Y, et al. (2013) Reduced mitochondrial ros, enhanced antioxidant defense, and distinct age-related changes in oxidative damage in muscles of long-lived peromyscus leucopus. *Am J Physiol Regul Integr Comp Physiol* 304:R343–R355.
27. Salway KD, Gallagher EJ, Page MM, Stuart JA (2011) Higher levels of heat shock proteins in longer-lived mammals and birds. *Mechanisms of Ageing and Development* 132(287—297).
28. Stadtman E (1992) Protein oxidation and aging. *Science* 257:1220–1224.
29. Borkovich KA, Farrelly FW, Finkelstein, D. B. Taulien J, Lindquist S (1989) hsp82 is an essential protein that is required in higher concentrations for growth of cells at higher temperatures. *Mol Cell Biol.* 9(9):3919–3930.
30. Fredriksson A, Ballesteros M, Dukan S, Nystrom T (2006) Induction of the heat shock regulon in response to increased mistranslation requires oxidative modification of the malformed proteins. *Molecular Microbiology* 59:350–359.
31. Begasse ML, Leaver M, Vazquez F, Grill SW, Hyman AA (2015) Temperature dependence of cell division timing accounts for a shift in the thermal limits of c. elegans and c. briggsae. *Cell Reports* 10:647–653.
32. Stroustrup N, et al. (2016) The temporal scaling of caenorhabditis elegans ageing. *Nature* 530:103—-107.
33. Mayor U, Johnson CM, Daggett V, Fersht AR (2000) Protein folding and unfolding in microseconds to nanonseconds by experiment and simulation. *Proc. Natl. Acad. Sci., USA* 97(25):13518–13522.
34. Depuydt G, Shanmugam N, Rasulova M, Dhondt I, Braeckman B (2016) Increased protein stability and decreased protein turnover in the caenorhabditis elegans ins/igf-1 daf-2 mutant. *Journals of Gerontology Series a-Biological Sciences and Medical Sciences* 71:1553–1559.
35. Leuenberger P, et al. (2017) Cell-wide analysis of protein thermal unfolding reveals determinants of thermostability. *Science* 355(6327).

36. Sun L, et al. (2012) The lid domain of caenorhabditis elegans hsc70 influences atp turnover, cofactor binding and protein folding activity. *Plos One* 7:e33980.

37. Wang M, Herrmann C, Simonovic M, Szklarczyk D, von Mering C (2015) Version 4.0 of paxdb: Protein abundance data, integrated across model organisms, tissues, and cell-lines. *Proteomics* 15(18):3163–3168.